crystals

MDPI

Article

Effects of LiF-Addition on Sintering Behavior and Dielectric Response of $LaPO_4$ Ceramics at Microwave and Terahertz Frequency for LTCC Applications

Hu Li [1,2], Dongfeng Wang [2], Kainan Zhang [3], Weijia Guo [4], Xiaoyu Xu [2], Yanbin Zhang [2], Yan Sun [2], Xingqi Xu [2], Jialun Du [1], Haitao Wu [1,*], Guangbin Duan [2,*] and Zhenxing Yue [4,*]

1 Yantai Unviersity, Yantai 264005, China
2 School of Materials Science and Engineering, University of Jinan, Jinan 250022, China
3 School of Chemistry and Chemical Engineering, University of Jinan, Jinan 250022, China
4 State Key Laboratory of New Ceramics and Fine Processing, School of Materials Science and Engineering, Tsinghua University, Beijing 100084, China
* Correspondence: wuhaitao@ytu.edu.cn (H.W.); mse_duangb@ujn.edu.cn (G.D.); yuezhx@tsinghua.edu.cn (Z.Y.)

Abstract: This paper reports on the successful preparation of $LaPO_4$-x wt.% LiF (x = 0–5) ceramics using the traditional solid-state reaction method. The crystal structures, sintering behaviors, and dielectric response at microwave and terahertz frequencies were investigated. XRD results indicate that all the diffraction peaks were attributed to $LaPO_4$, and no secondary phase was observed. Rietveld refinement was conducted to analyze the variation of the crystal structure of $LaPO_4$-x wt.% LiF. SEM indicates that the addition of LiF significantly decreased the grain size while increasing the apparent density of the ceramics. When x = 3, the optimum microwave dielectric properties ε_r = 10.03, $Q \times f$ = 81,467 GHz, and τ_f = −43.79 ppm/°C were achieved in $LaPO_4$-3 wt.% LiF ceramic at 750 °C. The infrared reflectance spectrum and terahertz time-domain spectroscopy were analyzed and compared with the dielectric properties measured at microwave frequency to investigate the inherent dielectric response. The findings indicate that the dielectric constant attributed to ionic displacement polarization and oxygen vacancy is an essential factor affecting dielectric loss. Moreover, it is worth noting that the $LaPO_4$-3 wt.% LiF ceramic demonstrates excellent compatibility with silver powders, suggesting its immense potential as a dielectric material in LTCC applications.

Keywords: microwave dielectric properties; rare earth phosphates; Rietveld refinement; infrared reflectance spectrum; LTCC

check for updates

Citation: Li, H.; Wang, D.; Zhang, K.; Guo, W.; Xu, X.; Zhang, Y.; Sun, Y.; Xu, X.; Du, J.; Wu, H.; et al. Effects of LiF-Addition on Sintering Behavior and Dielectric Response of $LaPO_4$ Ceramics at Microwave and Terahertz Frequency for LTCC Applications. *Crystals* **2023**, *13*, 1035. https://doi.org/10.3390/cryst13071035

Academic Editor: Francisco M. Morales

Received: 22 May 2023
Revised: 22 June 2023
Accepted: 25 June 2023
Published: 29 June 2023

1. Introduction

With the development of wireless communication and the arrival of the 5G era, the demand for high–speed, high-capacity wireless technology in 5G communications is soaring [1–3]. In the future communication field, the operating frequency will be expanded to micron and millimeter waves. Microwave dielectric ceramics, which are essential components in passive devices, have garnered more attention due to their exceptional performance. The main parameters to measure the properties of microwave dielectric ceramics are the dielectric constant (ε_r), quality factor ($Q \times f$), and temperature coefficient (τ_f). Among these, ε_r is a physical quantity that characterizes polarizability. High-frequency communication is characterized by low signal delay and therefore requires a low dielectric constant in the material. $Q \times f$ described the dielectric loss of materials [4]. A high-quality factor means high signal quality. τ_f determines the stability of signals and requires a value near zero to ensure operating stability at work. In addition, to realize the device application of materials, low-temperature co-firing technology (LTCC) is necessary [5–9].

Rare-earth phosphates exist in crystals of two structures (monazite and xenotime). Therein, high atomic masses (La, Ce, Pr, Nd, Sm, and Eu) tend to form the monazite phase,

and other elements (Tb, Dy, Ho, Er, Tm, Yb, and Y) form the xenotime phase. However, the researcher mainly focused on other properties, such as luminescence and catalysis [10–12]. Narasimha et al. reported the microwave dielectric properties of $LaPO_4$ [13]. Cho et al. published the microwave dielectric properties of a series of rare-earth phosphates [14]. $LaPO_4$ ceramic exhibits excellent microwave dielectric properties of ε_r = 10.4, $Q \times f$ = 64,556 GHz, and τ_f = −56.2 ppm/°C with a sintering temperature of 1400 °C and would be a good candidate for future 5G communications. However, the high sintering temperature impeded the application at the passive device terminal. Therefore, reducing the sintering temperature is meaningful work.

It is well known that the search for new ceramic systems or the addition of sintering aids can be effective in reducing sintering temperatures. Li-based ceramics usually have a low sintering temperature. Kamutzki et al. [15] successfully prepared $LiCrSi_2O_6$ microwave dielectric ceramics at low temperatures by applying the plasma spark sintering method, obtaining relatively excellent dielectric properties. However, the latter is easier to achieve than the option of adding a sintering aid.

As the universal sintering assistant, LiF has been used in this paper. By adding LiF to the $BaFe_{0.5}Nb_{0.5}O_3$ ceramic system, Intatha et al. [16] successfully reduced the sintering temperature and improved the sintering characteristics of the ceramics. Song et al. [17] synthesized $SrWO_4$−2 wt.% LiF ceramic at 850 °C by the traditional solid phase reaction method with excellent microwave dielectric properties of ε_r = 9.03 and $Q \times f$ = 47,830 GHz. Hao et al. [18] prepared Li_2TiO_3−2.5 wt.% LiF ceramic with excellent microwave dielectric properties of ε_r = 24.01, $Q \times f$ = 75,500 GHz, and τ_f = −36.2 ppm/°C at 950 °C and exhibited good compatibility with Ag. However, adding LiF to $LaPO_4$ ceramic to reduce the sintering temperature has not been reported.

This article presents the preparation and investigation of $LaPO_4$-x wt.% LiF (x = 0–5) in terms of crystal structure, sintering behaviors, and dielectric properties at microwave and terahertz frequencies. The phase composition, crystal parameters, and sintering behaviors were investigated using XRD, SEM, Rietveld refinement, and apparent density. The infrared reflectance spectrum and terahertz time-domain spectroscopy investigated the intrinsic dielectric mechanism. In addition, the compatibility of samples with Ag has been analyzed.

2. Experimental Procedure

The $LaPO_4$-x wt.% LiF (x = 0, 1, 2, 3, 4, and 5) system was prepared by the traditional solid-state reaction method. High-purity powders of La_2O_3 (99.99%), $NH_4H_2PO_4$ (99%), and LiF (99%) as the primary raw materials were weighted stoichiometrically. The raw powders were mixed with zirconium balls and alcohol for 24 h. Then the slurry was dried in an oven at 80 °C and passed through a 60-mesh screen. The dried powders were calcined at 1200 °C to form the main crystal phase. Whereafter, LiF was added as a sintering aid and for secondary ball milling. Before being pressed into a pellet with a diameter of 10 mm and a height of 6 mm. To bind the pellets, 12 wt.% paraffin was added. Finally, the pellets were sintered with a heating rate of 5 °C/min.

The phase composition of the sample was identified using an X-ray diffractometer (Model D/MAX-B, Rigaku Co., Tokyo, Japan) at room temperature with Cu Kα radiation. The signals were collected in the range of 10°–80°. Archimedes' drainage method was carried out to measure the apparent density of the samples. Scanning electron microscopy (S-4800, Hitachi, Tokyo, Japan) was implemented to observe the microstructure. The microwave dielectric properties (ε_r, $Q \times f$, and τ_f) of the samples were measured by a network analyzer (3656D, Ceyear Co., Qingdao, China) with the Hakki-Coleman method [19]. The ε_r and τ_f were determined by the parallel plate method, and the $Q \times f$ was determined by the resonant cavity method. The temperature coefficient can be calculated using Equation (1).

$$\tau_f = \frac{f_2 - f_1}{(T_2 - T_1) \times f_1} \quad (1)$$

where the resonant frequencies f_1 and f_2 are measured at T_1 (25 °C) and T_2 (85 °C), respectively. The infrared reflectance spectrum was measured using a far infrared spectrometer (FTIR, Bruker IFS66v, Bruker Optics, Ettlingen, Germany) at the National Synchrotron Radiation Laboratory. The terahertz time-domain spectroscopy was measured by a THz-TD spectrometer (Z3, Zomega, Plano, TX, USA) in the State Key Laboratory of New Ceramics and Fine Technology, Tsinghua University [20–22]. The dielectric properties and loss in the terahertz band are calculated as follows: Equations (2)–(7) [23–25].

$$\varepsilon'(\omega) - \mathrm{i}\varepsilon''(\omega) = [\mathrm{n}(\omega) - \mathrm{ik}(\omega)]^2 \tag{2}$$

$$\mathrm{n}^*(\omega) = \mathrm{n}(\omega) - \mathrm{ik}(\omega) \tag{3}$$

$$\alpha(\omega) = \frac{2\omega \mathrm{k}(\omega)}{v} \tag{4}$$

$$k(\omega) = \frac{\alpha(\omega)\cdot\lambda}{4\pi} \tag{5}$$

$$\varepsilon = n^2(\omega) - \left[\frac{\alpha(\omega)\cdot\lambda}{4\pi}\right]^2 \tag{6}$$

$$\tan\delta = \frac{\varepsilon''(\omega)}{\varepsilon'(\omega)} = \frac{n(\omega) - \alpha(\omega)\cdot\lambda}{2\pi}\left\{n^2(\omega) - \left[\frac{\alpha(\omega)\cdot\lambda}{4\pi}\right]^2\right\} \tag{7}$$

where $n^*(\omega)$ is the complex refractive index at terahertz frequency, $n(\omega)$ is the index of refraction, $k(\omega)$is the coefficient of extinction, v is the propagation speed of an electromagnetic wave at terahertz, ω is the frequency of Angle, and $\alpha(\omega)$ is the coefficient of absorption.

3. Results and Discussion

Figure 1 shows the XRD diffraction pattern of $LaPO_4$-x wt.% LiF ceramic. The figure's diffraction peaks are consistent with the standard PDF card (PDF#83–0651), indicating that the crystal structure is a single monoclinic structure with a space group of $P2_1/c$. The absence of the diffraction peak of the second phase demonstrates that the addition of LiF does not affect the formation of the $LaPO_4$ main stage.

Figure 1b shows that with increasing doping of LiF, the diffraction peaks corresponding to the (200) crystal orientations are shifted towards. According to the Bragg equation, the lattice parameters and cell volume change as the angle shifts. The lattice parameters and cell volume also change as the angle shifts; with increasing x, the cell volume increases from 306.115 $Å^3$ to 306.339 $Å^3$ as x increases.

Figure 2 exhibits the refined XRD data using Full Prof software (FullProf_Suite Windows (64 bits)). Table 1 summarizes lattice parameters and reliability factors. The smooth red line represents the difference between the measured and theoretical values, while the lower R-factors indicate that the refined results are reliable [26–28]. Figure 3 displays a single-unit cell diagram of $LaPO_4$ ceramic. The crystal cell comprises [LaO_9] polyhedrons and [PO_4] tetrahedrons. [LaO_9] and [PO_4] connect with oxygen along the b-axis. To intuitively understand the microscopic morphology of $LaPO_4$-x wt.% LiF ceramics.

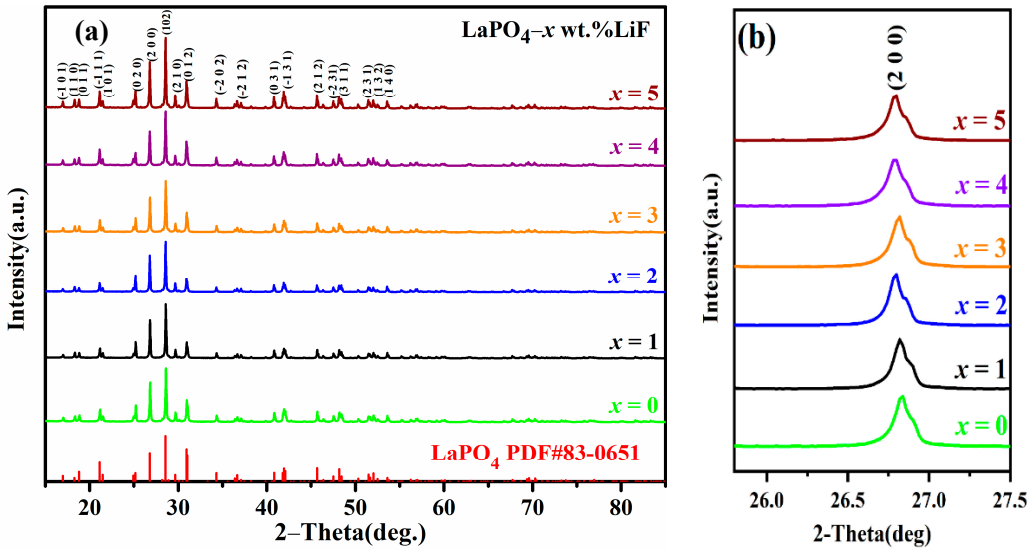

Figure 1. XRD pattern of the $LaPO_4$-*x* wt.% LiF ceramics at the optimal sintering temperatures. (**a**) overall X-ray diffraction pattern; (**b**) local XRD trends.

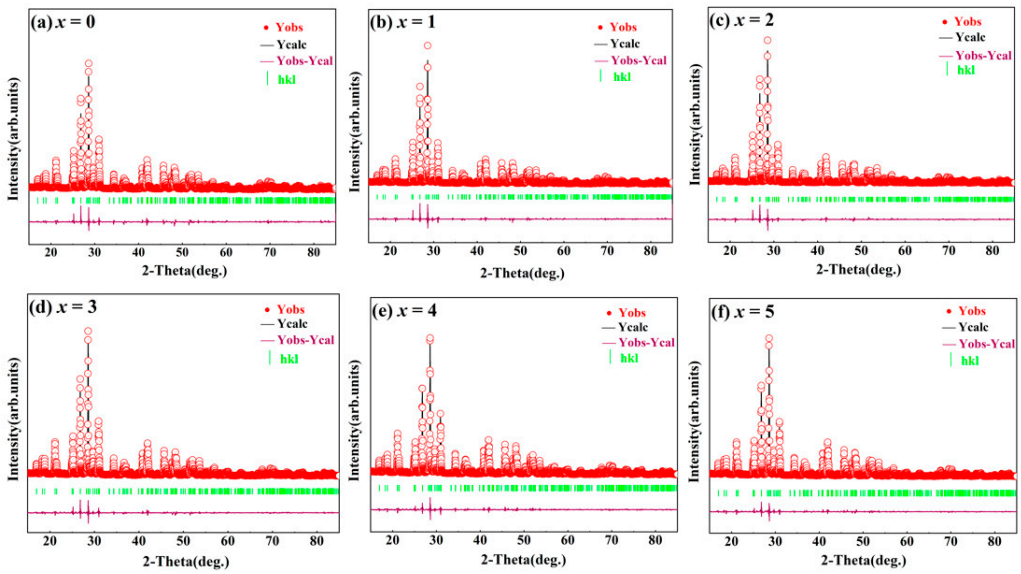

Figure 2. The refinement patterns of the $LaPO_4$-*x* wt.% LiF ceramics at the optimal sintering temperatures ((**a**–**f**) corresponding to 1400 °C, 900 °C, 900 °C, 750 °C, 750 °C, 750 °C).

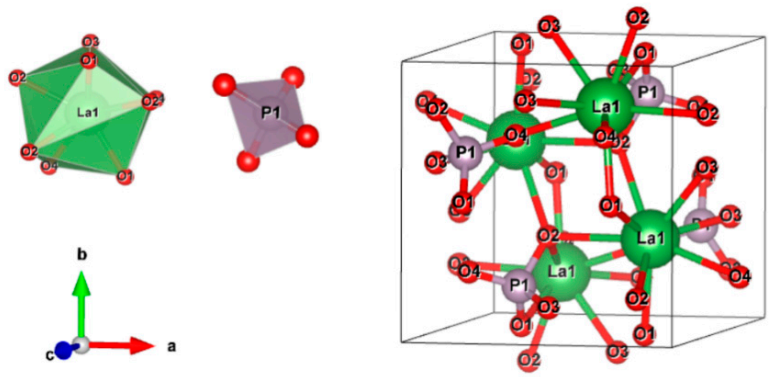

Figure 3. Unit cell diagram of the $LaPO_4$-3 wt.% LiF ceramic.

Table 1. The refinement patterns of the $LaPO_4$-*x* wt.% LiF ceramics at the optimal sintering temperatures.

	$x = 0$	$x = 1$	$x = 2$	$x = 3$	$x = 4$	$x = 5$
a (Å)	6.8358	6.8359	6.8368	6.8366	6.8367	6.8371
b (Å)	7.0728	7.0743	7.0749	7.0745	7.0746	7.0748
c (Å)	6.5058	6.5043	6.5070	6.5069	6.5068	6.5069
α (°)	90.000	90.000	90.000	90.000	90.000	90.000
β (°)	103.295	103.276	103.268	103.270	103.272	103.273
γ (°)	90.000	90.000	90.000	90.000	90.000	90.000
Z	4	4	4	4	4	4
V_m (Å^3)	306.115	306.233	306.337	306.307	306.310	306.339
R_p	10.60	10.70	11.50	9.42	9.12	9.08
R_{wp}	12.30	12.30	12.30	10.90	10.40	10.50
R_{ewp}	5.52	5.69	6.26	5.96	6.18	5.92
χ^2	2.23	2.16	1.96	1.82	1.68	1.77

Figure 4 displays the SEM image, which illustrates the changes in the apparent morphology of $LaPO_4$ ceramics with the increase in the amount of LiF. As shown in Figure 4a–e, when x = 1,2, the grain size is relatively large and the grain boundary is distinct. However, when $x \geq 3$, the grain size begins to refine, indicating that adding LiF is conducive to grain refinement. It is worth noting that due to the melting point of LiF at 845 °C, a part of LiF melts to form a liquid phase during the ceramic sintering process. When $x \geq 4$, grain boundaries begin to soften, and macroscopic defects such as pores between grains and cracks appear on the surface, which particularly impacts the apparent density and performance [29–31]. When the amount of LiF continues to increase, the sintering temperature does not change significantly. Excessive LiF exists on the grain surface in an amorphous state, and a small number of pores and cracks appear, which has an adverse effect on the densification of ceramics. This is consistent with the trend of relative density change and further indicates that an appropriate amount of LiF can effectively reduce the sintering temperature and porosity. Improve the relative density of ceramics.

Figure 5 shows the apparent density of $LaPO_4$-*x* wt.% LiF (x = 0–5) ceramics. Between 1250 °C and 1450 °C, the apparent density of the $LaPO_4$ ceramic matrix increases from 4.13 g/cm^{-1} to 4.40 g/cm^{-1} with the increase in temperature, indicating that temperature is an essential factor. Furthermore, the sintering interval of the $LaPO_4$-*x* wt.% LiF ceramics is 650 °C–1000 °C, meaning that the addition of LiF successfully reduces the sintering temperature of ceramics. The sintering temperature decreases further with the increase in LiF content. When x = 3, the temperature is reduced to 750 °C. At different x values, the apparent density increases first and then decrease. Figure 5b shows the relative density of ceramic samples. The shrinkage increases initially with the increase of x and reaches its maximum value at x = 3.

Figure 6 is the dielectric constant (ε_r) of $LaPO_4$-*x* wt.% LiF (x = 0–5) ceramics. As the sintering temperature increases, the ε_r first increases and then decreases. It takes x = 3 as an example. When the temperature increases from 700 °C to 750 °C, the ε_r increases from 7.08 to 10.03. However, as the temperature rises, the ε_r begins to decrease slowly. The ε_r is affected by several factors, such as dielectric polarization, porosity, and second equality [24,32,33]. However, the X-ray shows that the $LaPO_4$-*x* wt.% LiF (x = 0–5) ceramic is a single pure phase. The change in apparent density is the same as the dielectric constant, so the density is the main factor affecting the dielectric constant of $LaPO_4$ ceramics. Adding LiF reduces the sintering temperature and promotes the densification of ceramics. Therefore, as the temperature increases, giant permittivity is obtained. Still, when the temperature exceeds the optimal sintering temperature, the increase in grain size destroys the crystal structure, leading to a decrease in density and a consequent reduction in permittivity.

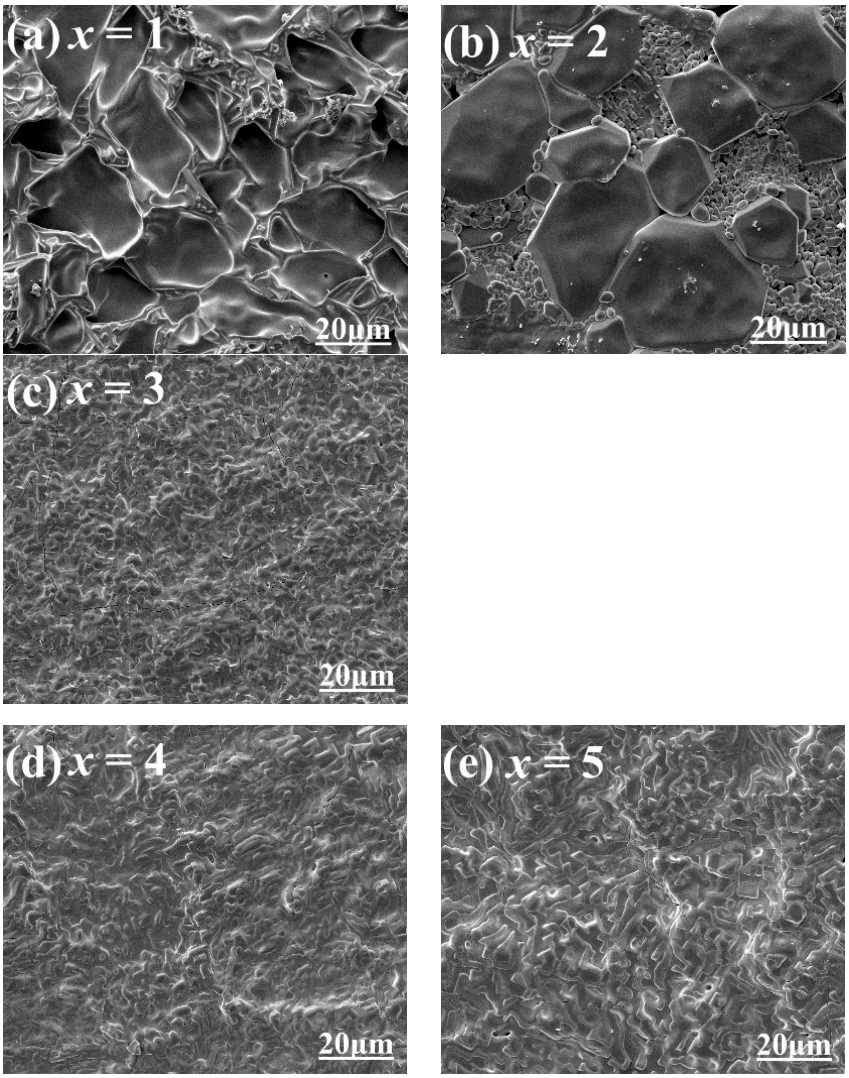

Figure 4. The morphology of the $LaPO_4$-*x* wt.% LiF ceramics as a function of the *x* values ((**a**–**e**) corresponding to 900 °C, 900 °C, 750 °C, 750 °C, 750 °C).

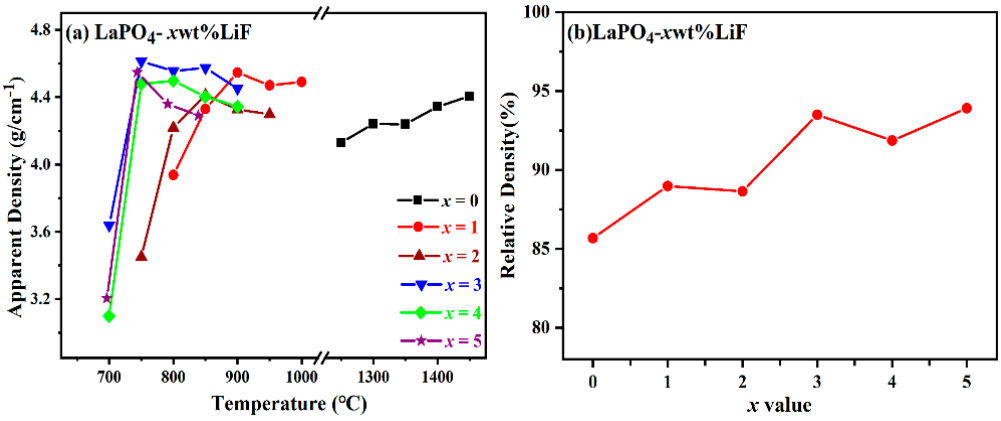

Figure 5. Density of the $LaPO_4$-*x* wt.% LiF ceramics as a function of the *x* values. (**a**) Apparent density; (**b**) relative density.

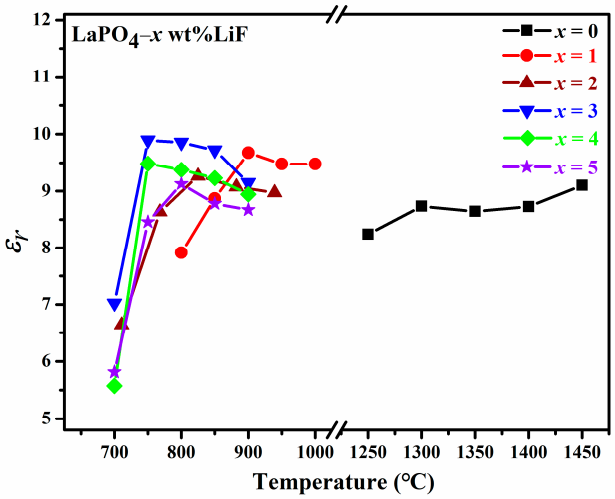

Figure 6. Dielectric constant (ε_r) of the $LaPO_4$-x wt.% LiF ceramics sintered at various temperatures.

Figure 7 is the quality factor ($Q \times f$) of $LaPO_4$-x wt.% LiF (x = 0–5) ceramics. The quality factor has the same variation as the dielectric constant. For instance, when x = 3, as an example. With the temperature increasing, the $Q \times f$ increases significantly from 15,946 GHz at 700 °C to 81,467 GHz at 750 °C, and the $Q \times f$ begins to decrease as the temperature continues to rise. Many factors affect the $Q \times f$. These factors fall into two categories: inherent losses and external losses. The lattice vibration mode and crystal structure influence the inherent losses [34,35]. The sintering additive effectively reduces the sintering temperature of $LaPO_4$ ceramics, but the phase composition is not affected. Thus, the main factor affecting the quality factor is density. Before reaching the optimum temperature point (750 °C), the increase in temperature is beneficial to reduce the number of pores in the ceramic, improve the density, and reduce the material loss inside the ceramic. As the temperature continues to rise, especially to 800 °C, several macroscopic cracks and pores make the interior loose, leading to the $Q \times f$ dropping to 68,791 GHz. The quality factor finally stabilizes within the range of 68,000 GHz to 77,000 GHz.

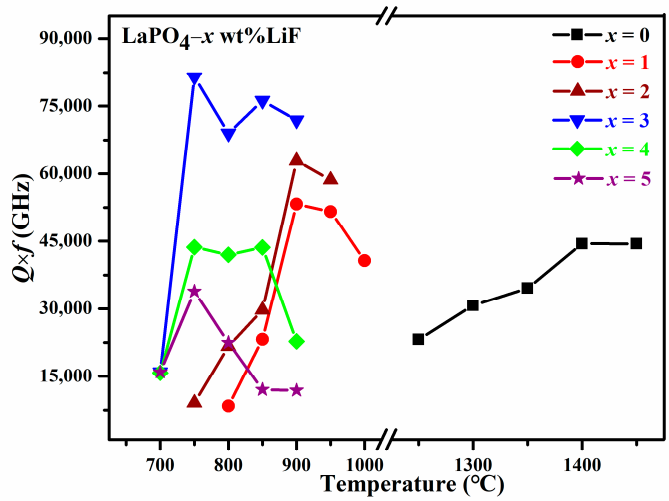

Figure 7. Quality factor ($Q \times f$) of the $LaPO_4$-x wt.% LiF ceramics sintered at various temperatures.

The temperature coefficient characterizes the thermal stability of materials. Figure 8 summarizes the trend of the temperature coefficient. The temperature coefficients are all negative, and the change of x and τ_f does not change significantly. It fluctuates between −46.40 ppm/°C and −34.71 ppm/°C, indicating that adding LiF has little effect on the temperature coefficient. Table 2 shows the microwave dielectric properties of $LaPO_4$-x wt.% LiF ceramics. In conclusion, when x = 3, the optimum microwave dielectric

properties of $LaPO_4$-x wt.% LiF ceramics are T = 750 °C, ε_r = 10.03, $Q \times f$ = 81,467 GHz, and τ_f = −43.79 ppm/°C.

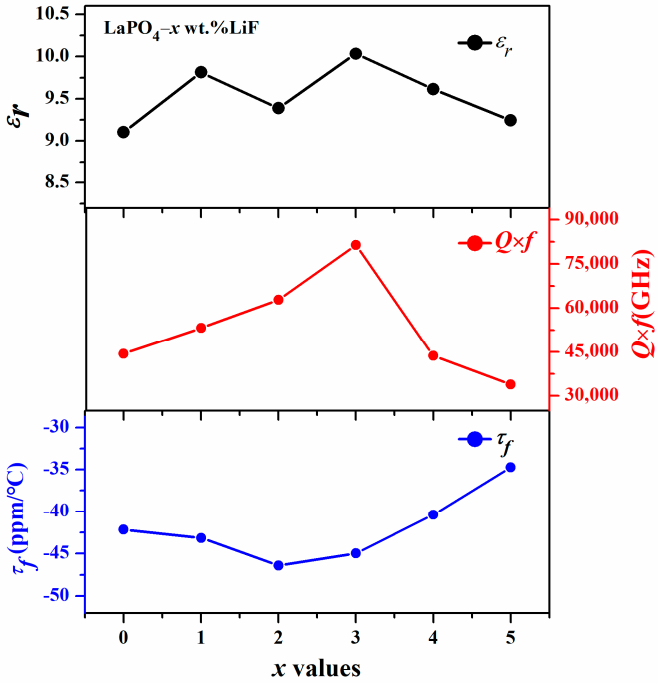

Figure 8. (τ_f) of the $LaPO_4$-x wt.% LiF ceramics at various temperatures.

Table 2. List of the microwave dielectric properties of the $LaPO_4$-x wt.% LiF ceramics.

Composition	S.T (°C)	ε_r	$Q \times f$ (GHz)	τ_f (ppm/°C)
$x = 0$	1400	8.73	44,449	−42.18
$x = 1$	900	9.81	53,247	−43.14
$x = 2$	900	9.19	62,844	−46.40
$x = 3$	750	10.04	81,467	−43.79
$x = 4$	750	9.61	43,674	−40.41
$x = 5$	750	8.56	33,873	−34.72

Infrared spectroscopy is an effective technique for characterizing the dielectric loss and response of ceramics. Figure 9a displays the fit of the infrared reflectance spectrum, obtained using the Reffit software and the classical resonator model with three parameters. The fitted values are in good agreement with the measured values. The complex permittivity (ε^*) and reflectance (R) can be calculated using Equations (8) and (9) in the harmonic oscillator mode [36,37]:

$$\varepsilon^*(\omega) = \varepsilon' + \varepsilon'' = \varepsilon_\infty + \sum_{i=1}^{n} \frac{\omega_{pj}^2}{\omega_{oj}^2 - \omega^2 - i\gamma_j\omega} \tag{8}$$

$$R(\omega) = \left| \frac{1 - \sqrt{\varepsilon^*(\omega)}}{1 + \sqrt{\varepsilon^*(\omega)}} \right|^2 \tag{9}$$

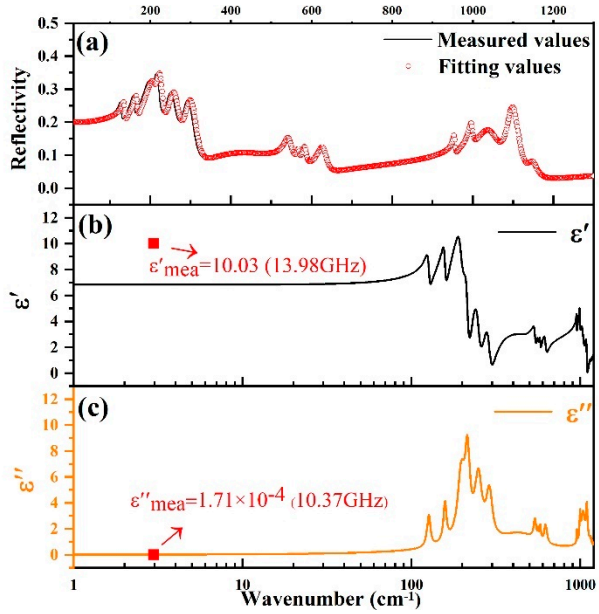

Figure 9. (**a**) Measured and fitted infrared reflectance spectrum curves; (**b**,**c**) complex permittivity of infrared spectra of the $LaPO_4$-3 wt.% LiF ceramic.

In the formula, ε_∞ is the optical permittivity, ω_{pj} and ω_{oj} are the plasma frequency and transverse frequency, respectively, γ_j is the damping factor, and i is the imaginary unit. Table 3 shows the vibration modes of 16 different phonons. The optical permittivity obtained by infrared spectrum fitting is 2.341. Figure 9 represents the real (ε') and imaginary (ε'') parts. The scattering of phonons and the overlap of peaks make the real part (ε' = 6.83) less than the measured dielectric constant (ε_r = 10.04) [37–39]. Figure 9c shows the observed dielectric loss (2.16×10^{-4}) in the same order of magnitude as the measured dielectric loss (1.72×10^{-4}), indicating that phonon vibration affects dielectric loss. Moreover, external factors such as porosity, density, and grain distribution also affect dielectric loss. Pores can be reduced or processes optimized to minimize losses.

Table 3. Phonon parameters obtained from the fitting of the $LaPO_4$-3 wt% LiF ceramic.

Mode	$LaPO_4$-3 wt.% LiF		ε_∞ = 2.341	
	ω_{oj}	ω_{pj}	γ_j	$\Delta\varepsilon_j$
1	126.5378	47.4173	7.1522	0.1404
2	157.7606	62.9653	8.1873	0.1593
3	197.1342	152.8907	23.5457	0.6015
4	214.3998	149.5696	16.9943	0.4867
5	248.9289	191.8766	30.0668	0.5941
6	288.8744	175.8852	29.1625	0.3707
7	456.4929	449.3217	332.2120	0.9688
8	537.1147	134.5086	22.1472	0.0627
9	561.8092	52.2352	7.7303	0.0086
10	577.8740	82.8326	11.3729	0.0205
11	621.9667	151.3773	26.1880	0.0592
12	951.8753	93.8768	6.2487	0.0097
13	994.1020	147.9418	11.1387	0.0221
14	1035.2952	432.4328	68.0378	0.1745
15	1091.1393	290.0738	26.4696	0.0707
16	1145.5237	128.5903	28.4676	0.0126

Infrared fitting results are easily limited by infrared pattern recognition. Terahertz time–domain spectroscopy technology investigates the effect of lattice vibration on properties. Figure 10 shows the dielectric response of $LaPO_4$-3 wt.% LiF sintered at 750 °C in the

frequency band of 0.5 THz~1.1 THz. The dielectric properties of the terahertz band are derived from the refractive index and extinction coefficient.

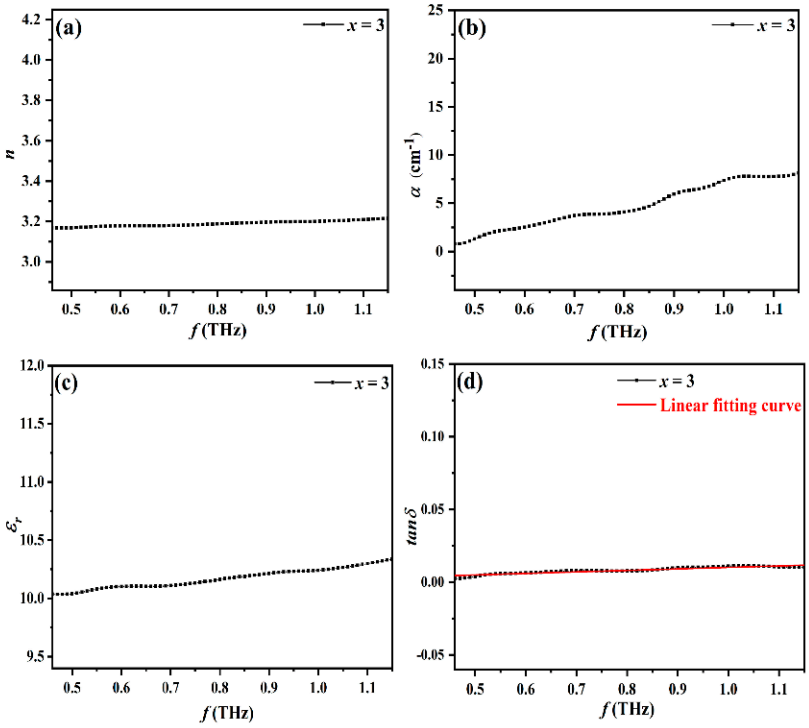

Figure 10. Optical and dielectric Properties of the $LaPO_4$-3 wt.% LiF ceramic in THz frequency band: (**a**) reflectance; (**b**) absorption coefficient; (**c**) dielectric constant; and (**d**) dielectric loss.

Figure 11 shows the change curve of the refractive index (n). The refractive index does not increase significantly with the increase in frequency and is stable between 3.17 and 3.21. The absorption coefficient (α) increases with the increase in frequency, which is associated with the unit volume polarizability. The dielectric constant which extrapolated from terahertz time-domain spectrum was in line with the value at microwave frequency [1,21,35]. At 7 GHz, the dielectric constant of ceramics is 10.03. At 0.5 THz, the dielectric constant of the ceramic is 10.04. Therefore, it can be inferred that the polarization mechanism of dielectric ceramic does not change in the terahertz frequency band, in which the ionic polarization is still dominant.

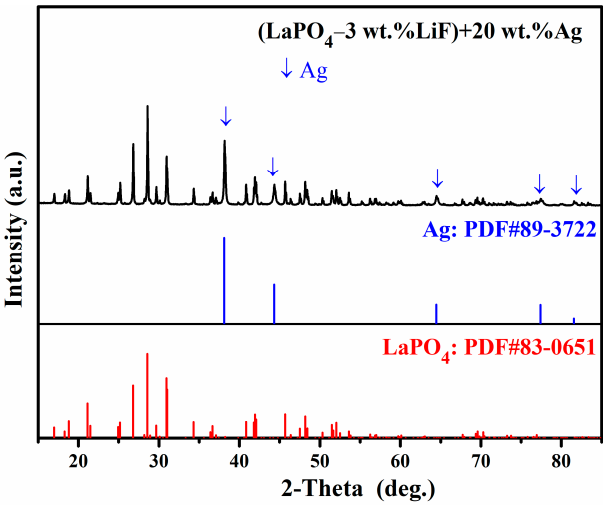

Figure 11. XRD pattern of the $LaPO_4$-3 wt.% LiF ceramic co-fired with Ag at 750 °C.

The fitted line in Figure 11 is the linear relationship between dielectric loss and frequency, and the slope of the matched line is 0.010, representing the vibration of the lattice. Considering the defect in the sample, it may be the oxygen vacancy that affects the dielectric loss. When x = 3, S.T. = 750 °C, the excellent optical and dielectric properties are: n = 3.17, ε_r = 10.03, α = 1.28 cm^{-1}, tan δ = 0.0039. Therefore, $LaPO_4$-3 wt.% LiF ceramics with low absorption coefficients and dielectric losses are optional for dielectric filters and lenses applied in the terahertz band.

The low-temperature co-firing ceramic (LTCC) technology has garnered significant attention due to its exceptional high-frequency characteristics, low energy consumption, and compact size. Among the various components of LTCC, the focus of research has been on LTCC materials. $LaPO_4$ ceramics have a high sintering temperature (1400 °C). Adding 3 wt.% LiF reduces the sintering temperature to 750 °C and has excellent dielectric properties. In this study, 20 wt.% Ag powder (10 μm) and $LaPO_4$-3 wt.% LiF ceramic powder at 750 °C are mixed and co-fired at 750 °C for 2 h. Figure 11 shows the XRD results. The results show that no chemical reaction occurs after co-firing $LaPO_4$-3 wt.% LiF ceramic and Ag, and the co-firing is a success, which provides a new idea for the future application of LTCC [29].

4. Conclusions

In this paper, the $LaPO_4$-x wt.% LiF (x = 0~5) ceramics are prepared by the traditional solid-state reaction method, and the microwave dielectric properties at different frequency bands are studied. The XRD patterns show that the ceramics crystallized in single phase $LaPO_4$, no secondary phase observed. Rietveld refinement by using Fullprof software. The results show that the crystal structure of the ceramics is monoclinic and that the phase composition of the mixture has not changed. LiF exists in the liquid phase and fills the void in ceramic. Therefore, with the increase of LiF, the relative density of ceramic is greatly improved compared with the matrix, the sintering temperature reduces to 750 °C, and the quality factor rises to 81,466 GHz. The dielectric constant increases by 10.03, and the temperature coefficient is −43.78 ppm/°C (x = 3). In the microwave frequency band, the ion shift polarization determines the dielectric constant, and the dielectric loss is mainly due to the lattice vibration. In the THz frequency band, the main factor affecting the dielectric constant is the ion displacement polarization, while the oxygen vacancy is the main factor affecting the dielectric loss. At 750 °C, $LaPO_4$-3 wt.% LiF ceramic powder does not react with Ag, and the co-firing is successful, indicating that $LaPO_4$-x wt.% LiF ceramic is an alternative material for future LTCC technology.

Author Contributions: Methodology, investigation, data curation, writing—original draft, and writing—reviewing and editing, H.L.; software and validation, D.W.; investigation, K.Z., W.G., J.D., X.X. (Xiaoyu Xu), Y.Z., Y.S. And X.X. (Xingqi Xu); supervision, resources, project administration, and funding acquisition, H.W., G.D. and Z.Y. All authors have read and agreed to the published version of the manuscript.

Funding: National Natural Science Foundation (No. 51972143).

Data Availability Statement: The data and materials supporting this study's findings are available from the corresponding author upon reasonable request.

Acknowledgments: H. Wu thanks the National Natural Science Foundation (No. 51972143). The authors are also thankful to Zeming Qi and Chuansheng Hu of the IR Beamline Workstation of the National Synchrotron Radiation Laboratory (NSRL) for the IR measurements.

Conflicts of Interest: The authors declare no conflict of interest.

References

1. Liang, Z.; Zhang, Y.; Wu, J.; Lu, B.; Yang, Y.; Zhang, H.; Li, J. Glass-free $CaMg_{0.9-x}Li_{0.2}Mn_xSi_2O_6$ ceramics with enhanced dielectric properties for microwave and THz frequency applications. *Ceram. Int.* **2022**, *48*, 24091–24099. [CrossRef]
2. Guo, H.H.; Fu, M.S.; Zhou, D.; Du, C.; Wang, P.J.; Pang, L.X.; Liu, W.F.; Sombra, A.S.B.; Su, J.Z. Design of a High-Efficiency and -Gain Antenna Using Novel Low-Loss, Temperature-Stable $Li_2Ti_{1-x}(Cu_{1/3}Nb_{2/3})_xO_3$ Microwave Dielectric Ceramics. *ACS Appl. Mater. Interfaces* **2021**, *13*, 912–923. [CrossRef] [PubMed]
3. Yang, H.; Zhang, S.; Yang, H.; Wen, Q.; Yang, Q.; Gui, L.; Zhao, Q.; Li, E. The latest process and challenges of microwave dielectric ceramics based on pseudo phase diagrams. *J. Adv. Ceram.* **2021**, *10*, 885–932. [CrossRef]
4. Bao, J.; Zhang, Y.; Kimura, H.; Wu, H.; Yue, Z. Crystal structure, chemical bond characteristics, infrared reflection spectrum, and microwave dielectric properties of $Nd_2(Zr_{1-x}Ti_x)_3(MoO_4)_9$ ceramics. *J. Adv. Ceram.* **2023**, *12*, 82–92. [CrossRef]
5. Guo, W.; Ma, Z.; Luo, Y.; Chen, Y.; Yue, Z.; Li, L. Structure, defects, and microwave dielectric properties of Al-doped and Al/Nd co-doped $Ba_4Nd_{9.33}Ti_{18}O_{54}$ ceramics. *J. Adv. Ceram.* **2022**, *11*, 629–640. [CrossRef]
6. Feng, C.; Zhou, X.; Tao, B.; Wu, H.; Huang, S. Crystal structure and enhanced microwave dielectric properties of the $Ce_2[Zr_{1-x}(Al_{1/2}Ta_{1/2})_x]_3(MoO_4)_9$ ceramics at microwave frequency. *J. Adv. Ceram.* **2022**, *11*, 392–402. [CrossRef]
7. Li, F.; Tang, Y.; Li, J.; Fang, W.; Ao, L.; Wang, Y.; Zhao, X.; Fang, L. Effect of A-site cation on crystal structure and microwave dielectric properties of AGe_4O_9 (A = Ba, Sr) ceramics. *J. Eur. Ceram. Soc.* **2021**, *41*, 4153–4159. [CrossRef]
8. Chen, J.; Fang, W.; Ao, L.; Tang, Y.; Li, J.; Liu, L.; Fang, L. Structure and chemical bond characteristics of two low-εr microwave dielectric ceramics $LiBO_2$ (B = Ga, In) with opposite τf. *J. Eur. Ceram. Soc.* **2021**, *41*, 3452–3458. [CrossRef]
9. Qian, J.; Li, G.; Zhu, K.; Ge, G.; Shi, C.; Liu, Y.; Yan, F.; Li, Y.; Shen, B.; Zhai, J.; et al. High Energy Storage Performance and Large Electrocaloric Response in $Bi_{0.5}Na_{0.5}TiO_3$-$Ba(Zr_{0.2}Ti_{0.8})O_3$ Thin Films. *ACS Appl. Mater. Interfaces* **2022**, *14*, 54012–54020. [CrossRef]
10. Norby, T.; Christiansen, N. Proton conduction in Ca- and Sr-substituted $LaPO_4$. *Solid State Ion.* **1995**, *77*, 240–243. [CrossRef]
11. Rambabu, U.; Amalnerkar, D.P.; Kale, B.B.; Buddhudu, S. Optical properties of $LnPO_4$:Tb^{3+} (Ln = Y, La and Gd) powder phosphors. *Mater. Chem. Phys.* **2001**, *70*, 401–408. [CrossRef]
12. Onoda, H.; Nariai, H.; Maki, H.; Motooka, I. Addition of Urea or Biuret on Synthesis of Rhabdophanetype Neodymium and Cerium Phosphates. *J. Mater. Synth. Process.* **2002**, *10*, 121–126. [CrossRef]
13. Narasimha, B.; Chouduary, R.N.P.; Rao, K.V. Dielectric properties of $LaPO_4$ ceramics. *J. Mater. Sci.* **1988**, *23*, 1416–1418. [CrossRef]
14. Cho, I.-S.; Choi, G.K.; An, J.-S.; Kim, J.-R.; Hong, K.S. Sintering, microstructure and microwave dielectric properties of rare earth orthophosphates, $RePO_4$ (Re=La, Ce, Nd, Sm, Tb, Dy, Y, Yb). *Mater. Res. Bull.* **2009**, *44*, 173–178. [CrossRef]
15. Kamutzki, F.; Schneider, S.; Müller, J.T.; Barowski, J.; Klimm, D.; Gurlo, A.; Hanaor, D.A.H. Low-Temperature Sintering of Low-Loss Millimeter-Wave Dielectric Ceramics Based on Li-Kosmochlor, $LiCrSi_2O_6$. *Phys. Status Solidi A* **2023**, *220*, 1–11. [CrossRef]
16. Intatha, U.; Eitssayeam, S.; Pengpat, K.; MacKenzie, K.J.D.; Tunkasiri, T. Dielectric properties of low temperature sintered LiF doped $BaFe_{0.5}Nb_{0.5}O_3$. *Mater. Lett.* **2007**, *61*, 196–200. [CrossRef]
17. Song, F.; Wang, X.; Lv, J.; An, Z.; Xu, Y.; Zhang, L.; Guo, H.; Zhou, D.; Zhou, H.; Shi, F. Lattice vibrational characteristics and structure-property relationships of $SrWO_{4-x}$ wt.% LiF (x = 0.5–3.0) microwave dielectric ceramics. *Ceram. Int.* **2022**, *49*, 9338–9345. [CrossRef]
18. Hao, Y.-Z.; Yang, H.; Chen, G.-H.; Zhang, Q.-L. Microwave dielectric properties of Li_2TiO_3 ceramics doped with LiF for LTCC applications. *J. Alloys Compd.* **2013**, *552*, 173–179. [CrossRef]
19. Jerzy, K.; Derzakowski, K.; Riddle, B.; Baker-Jarvis, J. A dielectric resonator for measurements of complex permittivity of low loss dielectric materials as a function of temperature. *Meas. Sci. Technol.* **1998**, *9*, 1751–1756.
20. Guo, W.; Ma, Z.; Chen, Y.; Lu, Y.; Yue, Z. Lattice dynamics and terahertz response of microwave dielectrics: A case study of Al-doped $Ca_{0.6}Sm_{0.27}TiO_3$ ceramics. *J. Eur. Ceram. Soc.* **2022**, *42*, 4953–4961. [CrossRef]
21. Luo, W.; Li, L.; Yu, S.; Li, J.; Zhang, B.; Qiao, J.; Chen, S. Bond theory, terahertz spectra, and dielectric studies in donor-acceptor (Nb-Al) substituted $ZnTiNb_2O_8$ system. *J. Am. Ceram. Soc.* **2019**, *102*, 4612–4620. [CrossRef]
22. Zhou, X.; Liu, L.; Sun, J.; Zhang, N.; Sun, H.; Wu, H.; Tao, W. Effects of $(Mg_{1/3}Sb_{2/3})^{4+}$ substitution on the structure and microwave dielectric properties of $Ce_2Zr_3(MoO_4)_9$ ceramics. *J. Adv. Ceram.* **2021**, *10*, 778–789. [CrossRef]
23. Pupeza, I.; Wilk, R.; Koch, M. Highly accurate optical material parameter determination with THz time-domain spectroscopy. *Opt. Express* **2007**, *15*, 4335–4350. [CrossRef] [PubMed]
24. Ruan, X.; Chan, C.H. Terahertz free-space dielectric property measurements using time- and frequency-domain setups. *Int. J. RF Microw. Comput. Aided Eng.* **2019**, *29*, e21839. [CrossRef]
25. Huang, J.B.; Yang, B.; Yu, C.Y.; Zhang, G.F.; Xue, H.; Xiong, Z.X.; Viola, G.; Donnan, R.; Yan, H.X.; Reece, M.J. Microwave and terahertz dielectric properties of $MgTiO_3$–$CaTiO_3$ ceramics. *Mater. Lett.* **2015**, *138*, 225–227. [CrossRef]
26. Bao, J.; Du, J.; Liu, L.; Wu, H.; Zhou, Y.; Yue, Z. A new type of microwave dielectric ceramic based on K_2O–SrO–P_2O_5 composition with high quality factor and low sintering temperature. *Ceram. Int.* **2022**, *48*, 784–794. [CrossRef]
27. Xiao, E.C.; Cao, Z.; Li, J.; Li, X.H.; Liu, M.; Yue, Z.; Chen, Y.; Chen, G.; Song, K.; Zhou, H.; et al. Crystal structure, dielectric properties, and lattice vibrational characteristics of LiNiPO4 ceramics sintered at different temperatures. *J. Am. Ceram. Soc.* **2019**, *103*, 2528–2539. [CrossRef]

28. Xing, C.; Li, J.; Wang, J.; Chen, H.; Qiao, H.; Yin, X.; Wang, Q.; Qi, Z.M.; Shi, F. Internal Relations between Crystal Structures and Intrinsic Properties of Nonstoichiometric Ba1+ xMoO_4 Ceramics. *Inorg. Chem.* **2018**, *57*, 7121–7128. [CrossRef]
29. An, Z.; Lv, J.; Wang, X.; Xu, Y.; Zhang, L.; Shi, F.; Guo, H.; Zhou, D.; Liu, B.; Song, K. Effects of LiF additive on crystal structures, lattice vibrational characteristics and dielectric properties of $CaWO_4$ microwave dielectric ceramics for LTCC applications. *Ceram. Int.* **2022**, *48*, 29929–29937. [CrossRef]
30. Chen, J.; Fang, W.; Tang, Y.; Jie, L.; Fang, L. Effects of LiF addition on the densification and microwave dielectric properties of $LiInO_2$ ceramics. *Ceram. Int.* **2021**, *47*, 28960–28967. [CrossRef]
31. Zhang, Y.H.; Sun, J.J.; Dai, N.; Wu, Z.C.; Wu, H.T.; Yang, C.H. Crystal structure, infrared spectra and microwave dielectric properties of novel extra low-temperature fired $Eu_2Zr_3(MoO_4)_9$ ceramics. *J. Eur. Ceram. Soc.* **2019**, *39*, 1127–1131. [CrossRef]
32. Parvez Ahmad, M.D.; Venkateswara Rao, A.; Suresh Babu, K.; Narsinga Rao, G. Effect of carbon-doping on structural and dielectric properties of zinc oxide. *J. Adv. Dielectr.* **2020**, *10*, 2050017. [CrossRef]
33. Diao, C.-L.; Wang, C.-H.; Luo, N.-N.; Qi, Z.-M.; Shao, T.; Wang, Y.-Y.; Lu, J.; Shi, F.; Jing, X.-P.; Ching, W.Y. First-Principle Calculation and Assignment for Vibrational Spectra of $(Mg_{1/2}W_{1/2})O_3$ Microwave Dielectric Ceramic. *J. Am. Ceram. Soc.* **2013**, *96*, 2898–2905. [CrossRef]
34. Tang, Y.; Zhang, Z.; Li, J.; Xu, M.; Zhai, Y.; Duan, L.; Su, C.; Liu, L.; Sun, Y.; Fang, L. $A_3Y_2Ge_3O_{12}$ (A = Ca, Mg): Two novel microwave dielectric ceramics with contrasting τf and Q × f. *J. Eur. Ceram. Soc.* **2020**, *40*, 3989–3995. [CrossRef]
35. Luo, Y.; Guo, W.; Chen, Y.; Zhang, J.; Yue, Z. Thermally-stimulated defect relaxations and microwave/terahertz dielectric response of La,Al co-doped (Ba,Sr)$La_4Ti_4O_{15}$ ceramics. *J. Eur. Ceram. Soc.* **2021**, *41*, 158–164. [CrossRef]
36. Shi, F.; Dong, H. Correlation of crystal structure, dielectric properties and lattice vibration spectra of $(Ba_{1-x}Sr_x)(Zn_{1/3}Nb_{2/3})O_3$ solid solutions. *Dalton. Trans.* **2011**, *40*, 6659–6667. [CrossRef]
37. Diao, C.-L.; Wang, C.-H.; Luo, N.-N.; Qi, Z.-M.; Shao, T.; Wang, Y.-Y.; Lu, J.; Wang, Q.-C.; Kuang, X.-J.; Fang, L.; et al. First-principle calculation and assignment for vibrational spectra of $Ba(Mg_{1/3}Nb_{2/3})O_3$microwave dielectric ceramic. *J. Appl. Phys.* **2014**, *115*, 114103. [CrossRef]
38. Tian, H.; Zheng, J.; Liu, L.; Wu, H.; Kimura, H.; Lu, Y.; Yue, Z. Structure characteristics and microwave dielectric properties of $Pr_2(Zr_{1-x}Ti_x)_3(MoO_4)_9$ solid solution ceramic with a stable temperature coefficient. *J. Mater. Sci. Technol.* **2022**, *116*, 121–129. [CrossRef]
39. Zubkov, S.V.; Vlasenko, V.G.; Shuvaeva, V.A.; Shevtsova, S.I. Structure and dielectric properties of solid solutions $Bi_7Ti_{4+x}W_xTa_{1-2x}O_{21}$ (x = 0–0.5). *Phys. Solid State* **2016**, *58*, 42–49. [CrossRef]